9-2010

Space-time properties of a boson-dressed fermion for the Yukawa model

R E. Wagner
Illinois State University

M R. Ware
Illinois State University

Q Su
Illinois State University

Rainer Grobe
Illinois State University

Space-time properties of a boson-dressed fermion for the Yukawa model

R. E. Wagner, M. R. Ware, Q. Su, and R. Grobe
Intense Laser Physics Theory Unit and Department of Physics, Illinois State University, Normal, Illinois 61790-4560, USA
(Received 24 February 2010; published 13 September 2010)

We analyze the interaction of fermions and bosons through a one-dimensional Yukawa model. We numerically compute the energy eigenstates that represent a physical fermion, which is a superposition of bare fermionic and bosonic eigenstates of the uncoupled Hamiltonian. It turns out that even fast bare fermions require only low-momentum dressing bosons, which attach themselves to the fast fermion through quantum correlations. We compare the space-time evolution of a physical fermion with that of its bare counterpart and show the importance of using dressed observables. The time evolution of the center of mass as well as the wave packet's spatial width suggests that the physical particle has a lower mass than the sum of the masses of its bare constituents. The numerically predicted dressed mass agrees with that from lowest-order perturbation theory as well as with the renormalized mass obtained from the corresponding Feynman graphs. For a given momentum, this lower mass leads to a faster physical particle and a different relativistic spreading behavior of the wave packet.

DOI: 10.1103/PhysRevA.82.032108 PACS number(s): 03.65.−w, 03.70.+k

I. INTRODUCTION

In quantum electrodynamics the state of a physical particle such as an electron is thought of as a superposition of bare fermions and bare photons. Bare particles are described by the energy eigenstates of the uncoupled fermion-boson Hamiltonian and are not energy eigenstates of the coupled Hamiltonian [1–4]. As a result, an initial state describing a bare fermion and no bosons creates bosons as time evolves. Some of these created bosons escape to infinity, while others become "glued" to the fermion to form the new stable fermion-boson superposition state (the physical fermion) [5].

It is not precisely clear what role these dressing bosons [6,7] play with regard to the interaction of a physical fermion with its environment. For instance, when a physical fermion absorbs and re-emits a boson during Compton scattering, what role do the dressing bosons play? In the case of the Coulombic interaction between two fermions of equal or opposite charge, the dressing bosons are essentially believed to be mediators of force. To the best of our knowledge, a detailed analysis that compares the properties of bare and physical fermions and bosons with full space-time resolution is presently lacking.

The usual approach to quantum field theoretical questions is typically based on S matrices obtained from perturbative Feynman graphs. These predict the various static properties such as magnetic moments, cross sections, and energy levels or transition rates of hydrogen-like atoms. These predictions have been verified experimentally with astonishing accuracy. However, there are still many computational and even conceptual challenges to address the questions above. This is due in part to the technical and computational difficulties associated with mass renormalizations and various divergences but also to the conceptual difficulties of going beyond the usual asymptotic time analysis and visualizing the dynamics inside the interaction zone in a nonperturbative way.

We approach these questions by using numerical solutions based on a model version of the quantum field theory of interacting fermion-boson fields. The motivation for this alternative approach is threefold. First, we hope that it can lead to the discovery of dynamical mechanisms, based on coherence, spatial localization, and nonstationary states that are difficult to obtain with rate-based S-matrix methods. Second, this—in principle exact—approach will allow us to test the limitations and ranges of validity of the usual perturbative methods in QED. Third, as this is an alternative approach to QED, we might also hope to develop better and more intuitive ways of understanding and visualizing these processes.

In the long term we hope that quantum-field-theoretical model studies can provide a similar insight as numerical solutions to the Schrödinger and Dirac equations did in atomic and laser physics during the last two decades. For example, computer-aided visualizations of the processes inside the interaction region based on one-dimensional model systems have led to exciting advances in understanding and controlling the mechanisms leading to the single- and multielectron ionization dynamics in the multiphoton regime, strong-field stabilization, and the generation of higher harmonics.

In order to obtain some first insight into QED, in this work we use the Yukawa system that was introduced in the 1930s to model phenomenologically the strong nuclear force and the interaction of nucleons with π mesons. It is also an integral part of the standard model to describe the Higgs-fermion coupling [3]. The only difference between this system and the Hamiltonian for electrodynamics is that the vector photon is replaced by a scalar particle that can have a nonzero mass, leading to only attractive interfermionic forces. Furthermore, if we decouple the positrons and restrict the dynamics to one spatial dimension, the Yukawa system has no ultraviolet divergence. This makes it an ideal model system for us to develop the quantum-field-theoretical framework needed to visualize interacting fermion-boson systems with full space-time resolution [8]. In three recent works, we have used a quasi-non-relativistic version of the Yukawa system to test the predictions of the Greenberg-Schweber (recoil-free) approximation [1,9,10], to simulate the evolution of a bare particle into a physical particle by the generation of a cloud of dressing bosons that surrounds the fermion [5], and to examine the mutual coherence properties of bosons that were created by two spatially distinct regions of a single bare fermion state [11].

The paper is structured as follows. In Sec. II, we introduce the model system and discuss the computational aspects that make a nonperturbative analysis feasible; in Sec. III, we compare the space-time evolution of the bare fermionic wave packet with a dressed fermion that represents the actual physical particle. We finish with a brief discussion and an outlook on future work.

II. THE YUKAWA MODEL SYSTEM AND ITS NUMERICAL SOLUTION

We model the boson-fermion interaction with a Hamiltonian $\hat{H} = \hat{H}_0 + \hat{V}$ (in atomic units with $c = 137$ a.u. and $\hbar = 1$ a.u.), where

$$\hat{H}_0 = \int dp E_p \hat{b}_p^\dagger \hat{b}_p + \int dk \omega_k \hat{a}_k^\dagger \hat{a}_k, \tag{1a}$$

$$\hat{V} = \gamma c^{5/2} \int dp \int dk \Gamma(p,k) \hat{b}_{p+k}^\dagger \hat{b}_p (\hat{a}_k + \hat{a}_{-k}^\dagger). \tag{1b}$$

The fermionic and bosonic creation and annihilation operators fulfill the anticommutator and commutator relationships, $[\hat{b}_p, \hat{b}_{p'}^\dagger]_+ = \delta(p - p')$ and $[\hat{a}_k, \hat{a}_{k'}^\dagger]_- = \delta(k - k')$. The interaction-free energies for the fermions and bosons are denoted by $E_p \equiv \sqrt{[M^2c^4 + c^2p^2]}$ and $\omega_k \equiv \sqrt{[m^2c^4 + c^2k^2]}$, respectively. The coupling parameter γ has units of mass, and M and m denote the bare fermionic and bosonic masses. The coupling function $\Gamma(p,k)$ is the result of the scalar product among the Dirac spinors and acts as a natural cutoff function as it decreases with increasing momenta p and k. It is given by $\Gamma(p,k) \equiv [E_{p+k}E_p + M^2c^4 - p(p+k)c^2]^{1/2} (8\pi\omega_k E_{p+k} E_p)^{-1/2}$. As a side remark, we note that for a different functional form of $\Gamma(p,k)$ the same Hamiltonian can also be used to examine the interaction of charged bosons with neutral bosons. The operators in momentum space are related to the complex fermion field $\hat{\Psi}(x) \equiv (2\pi)^{-1/2} \int dp \hat{b}_p (2E_p)^{-1/2} [\sqrt{(E_p - cp)}, \sqrt{(E_p + cp)}]^T \exp(ipx)$, where we used Dirac matrices represented here in terms of the Pauli matrices, $\gamma^0 = \sigma_1$ and $\gamma^1 = i\sigma_2$. We also omitted the positronic part from $\hat{\Psi}(x)$. The real boson field is defined as $\hat{\varphi}(x) \equiv (2\pi)^{-1/2} \int dk c (2\omega_k)^{-1/2} \hat{a}_k \exp(ikx) + \text{H.c.}$ When expressed in terms of the field operators, the interaction Hamiltonian can be rewritten as $\hat{V} = \gamma c^{3/2} \int dx \hat{\bar{\Psi}}(x) \hat{\Psi}(x) \hat{\varphi}(x)$, showing that the interaction is local in the coordinate representation. The conjugate spinor $\hat{\bar{\Psi}}(x)$ is defined as $\hat{\Psi}^\dagger(x)\gamma^0$, where the dagger is the usual Hermitian conjugate. The entire Hilbert space can be spanned by the direct product of bare fermionic and bosonic states, defined as the energy eigenstates of the uncoupled Hamiltonian $\hat{H}_0$ in Eq. (1a). The dynamics is restricted due to the existence of two operators that commute with the Hamiltonian, associated with the conservation of the total number of fermions, $\int dp \hat{b}_p^\dagger \hat{b}_p$, and the total momentum, $\int dp p \hat{b}_p^\dagger \hat{b}_p + \int dk k \hat{a}_k^\dagger \hat{a}_k$. These operators lead to invariant subspaces that can reduce the analysis significantly [8].

In this work we focus on the subspace of a single fermion ($\int dp \hat{b}_p^\dagger \hat{b}_p = 1$), and if the states are arranged in blocks characterized by the total momentum quantum number $P = p + \int dk n_k k$, the Hamiltonian $\hat{H} = \hat{H}_0 + \hat{V}$ is block diagonal, where n_k denotes the occupation number of the k-momentum mode.

In order to make the Hamiltonian computationally feasible, we have discretized the spatial axis into $(2P + 1)$ numerical grid points for $n = -P, \ldots, P$, defined as $x_n = n\Delta x$, where the grid spacing $\Delta x \equiv L/(2P + 1)$ depends on the length of the numerical box, L. To be consistent, the corresponding bosonic and fermionic momenta have a range from $-K\Delta p$ to $K\Delta p$ and from $-P\Delta p$ to $P\Delta p$, respectively, where $\Delta p = 2\pi/L$ and K is the maximum bosonic momentum quantum number. If the maximum occupation number in each bosonic mode were limited to N, the Hilbert space becomes finite with a dimension of $(2P + 1)(N + 1)^{2K+1}$. As an example, if space were discretized into 41 points ($P = 20$), the bosons' momentum were restricted to only $K = 8$, and only a maximum of 3 bosons per mode were allowed, the Hamiltonian would still be represented by almost 4.9×10^{23} matrix elements. This would consume more than 10^{15} gigabytes of computer memory, which is clearly an unrealistic demand.

However, due to momentum conservation, the matrix can be diagonalized in the total momentum subspaces. The computer program was written in FORTRAN, and using a dynamical memory allocation of each subspace based on pointer variables, it is possible to calculate the dynamics based on a Hilbert space with up to 700,000 energy eigenstates if the maximum occupation number is optimized for each boson mode.

The state with the lowest energy E in each subspace (denoted below by $|P\rangle = |E_{\text{lowest}}\rangle$) is interpreted as the dressed state describing a physical fermion with sharp total momentum P and no physical boson. In the limit of $\gamma \to 0$, the state $|P\rangle$ returns to the bare state $|p, \{n_k = 0\}\rangle$ with momentum $p = P$ and no excess bosons. In the absence of any level crossings, this state can be easily identified numerically because it is associated with the lowest eigenenergy, as $E_p \leqslant E_{p-k} + \omega_k$ is valid for any p, k, M, and m. This inequality, however, is valid only if the energies take the relativistic form given by the expressions above. For example, in the nonrelativistic form (and for $k = p$ and $m = 0$), we can have $E_p = p^2/(2M) + Mc^2 > Mc^2 + cp$, and the energy-based identification of $|P\rangle$ would fail. It also turns out that for $\gamma \to 0$ the second-lowest-energy eigenstate in each momentum subspace approaches the state $|p, n_{k=0} = 1\rangle$ in which a single boson is in the zero-momentum state. Any further association of states with their bare quantum numbers, however, is in general more difficult for higher energy states, since it depends on the values of M, m, and Δp.

The state $|P\rangle$ is a superposition of bare energy eigenstates with several momenta p and several bare bosons. It is difficult to obtain analytical estimates of the composition of bare fermions and bosons in the state $|P\rangle$ for large coupling constants γ. However, for the special limit of the Greenberg-Schweber approximation [1,9,10] [$M \to \infty$ such that the bare fermion's energy does not depend on the momentum, $E_p = E$ and $\Gamma(p,k) = (4\pi\omega_k)^{-1/2}$], analytical estimates are available. For example, one can find $\langle P|\hat{a}_k^\dagger \hat{a}_k|P\rangle = \gamma^2 c^5 (2L\omega_k^3)^{-1}$, giving us a first indication that only low-k bosons contribute to the dressing.

It is also interesting to note that bare states with low boson momentum k contribute to the dressed state $|P\rangle$ (with large P) with more weight than states with larger boson momenta. This can be seen if we use the first-order perturbative expansion of the state $|P\rangle$,

$$|P\rangle = |p = P,\{n_k = 0\}\rangle + \gamma c^{5/2} \int dp' \Gamma(p', P - p') \times (E_P - E_{p'} - \omega_{P-p'})^{-1} |p', n_{k=P-p'} = 1\rangle, \quad (2)$$

and compute the scalar product with a single-boson state, $\langle P - k, n_k = 1|P\rangle = \gamma c^{5/2}\Gamma(P-k,k)(E_P - E_{P-k} - \omega_k)^{-1}$. This product takes its largest value for $k = 0$ and decreases with increasing k. As the dressing bosons are tied to the fermion's location and also its velocity, it is interesting that bosons with low bare momentum k can nevertheless move arbitrarily fast. In Appendix A, we show that the dressing bosons become "glued" to the bare fermion even independent of their momentum.

The general dependence of the energy eigenvalue on the total momentum P must be obtained numerically. An analytical estimate can be obtained if we assume that the fermion-boson coupling constant is sufficiently small, such that the eigenenergies can be approximated by their leading order in perturbation theory. Even though the unperturbed energies are doubly degenerate $[E(-p) = E(p)]$ due to the conserved total momentum, a 2×2 subspace diagonalization is not necessary. Using the usual expressions [12], we obtain

$$E(P,\gamma) = E(P) + \gamma^2 c^5 \int dk \Gamma(P,k)^2 [E(P) - E(P-k) - \omega_k]^{-1}. \quad (3)$$

Alternatively, using the standard perturbative renormalization technique based on the usual Feynman graphs, we can also calculate the corrected energies

$$E_{\rm ren}(P,\gamma) = [M_{\rm ren}(\gamma)^2 c^4 + c^2 P^2]^{1/2}, \quad (4)$$

where $M_{\rm ren}$ is the effective (renormalized) mass for the fermion. In Appendix B, we show the details of the corresponding derivation leading to

$$M_{\rm ren}(\gamma) = M - \gamma^2/(4\pi M)\Big[\ln(m/M) + \sqrt{(4M^2 - m^2)}/m\Big(\tan^{-1}[m/\sqrt{(4M^2 - m^2)}] + \tan^{-1}\{(2M^2 - m^2)/[m\sqrt{(4M^2 - m^2)}]\}\Big)\Big]. \quad (5)$$

Independent of the fermionic and bosonic bare masses M and m, the renormalized mass is always less than the fermionic mass, $M_{\rm ren}(\gamma) < M$. This is consistent with the fact that, for a given momentum P, the energy of the fermion decreases due to the dressing bosons. It also shows how the inertia (mass) of a compound (physical particle) can be less than the sum of the masses of the individual constituents separately. With decreasing boson mass m the renormalized mass decreases, while for $m \to \infty$ we have $M_{\rm ren} \to M$ for any γ.

The numerically obtained eigenvectors $|E\rangle$ and eigenvalues E permit us to compute the general time evolution of the quantum-field-theoretical state, via $|\Phi(t)\rangle = \int dE \exp(-iEt)\langle E|\Phi(t=0)\rangle|E\rangle$.

III. SPATIAL PROPERTIES OF THE PHYSICAL FERMION

In order to describe a spatially localized fermion, we use a Gaussian superposition of the dressed energy eigenstates $|P\rangle$,

$$|\Phi(t=0)\rangle = \int dP (2/\pi)^{1/4} \Delta^{1/2} \times \exp[-(P - P_0)^2 D^2] \exp[-iPx_0]|P\rangle, \quad (6)$$

where from now on the amplitude for the momentum state is abbreviated by $G(P)$. The parameters x_0, P_0, and Δ are the initial location, central momentum, and spatial width of the state, respectively. We note that the corresponding bare fermion would be given by the superposition of energy eigenstates of the uncoupled Hamiltonian $\hat{H}_0$, $|\Phi_{\rm bare}(t=0)\rangle = \int dp G(p)|p,\{n_k = 0\}\rangle$. As the bare basis states $|p,\{n_k = 0\}\rangle$ are not eigenstates of the full Hamiltonian for $\gamma \neq 0$, the time evolution of a bare localized state $|\Phi_{\rm bare}(t)\rangle$ is quite different than that of a physical localized state $|\Phi(t)\rangle$ and is unstable and generates bosons as it evolves in time [5].

The space-time evolution of the states $|\Phi(t)\rangle$ and $|\Phi_{\rm bare}(t)\rangle$ can be analyzed from the perspective of a single dressed particle or with respect to the properties of the underlying bare particles. The spatial distribution of the (bare) number density can be computed via $\langle\Phi|\hat{a}_x^\dagger \hat{a}_x|\Phi\rangle$ and $\langle\Phi|\hat{b}_x^\dagger \hat{b}_x|\Phi\rangle$, as discussed in many standard books [13–15]. Here $\hat{a}_x$ is the Fourier transform of the annihilation operator in momentum space, $\hat{a}_x \equiv (2\pi)^{-1/2}\int dk \hat{a}_k \exp(ikx)$, and correspondingly for $\hat{b}_x$. When integrated over the whole space, we obtain the total number of bosons, $N_b = \int dx \langle\hat{a}_x^\dagger \hat{a}_x\rangle$, such that the ratio $\langle\hat{a}_x^\dagger \hat{a}_x\rangle/N_b$ can be interpreted as the spatial probability density. Due to the conservation law of the fermion number mentioned above, we always have $\int dx \langle\hat{b}_x^\dagger \hat{b}_x\rangle = 1$.

The corresponding dressed properties are more difficult to determine. The physical operators can be defined by their action on the dressed states, $\hat{B}_P|P\rangle = |0\rangle$ and $\hat{B}_P^\dagger|0\rangle = |P\rangle$. Since in our special case here they are required to act only on the single fermion subspace and we need only expectation values of the combined product operator $\hat{B}_{P1}^\dagger \hat{B}_{P2}$, we can approximate these operators using the direct product of the numerically obtained eigenvectors as $\hat{B}_{P1}^\dagger \hat{B}_{P2} = |P_1\rangle\langle P_2|$. Similarly, we would define $\hat{B}_x = (2\pi)^{-1/2}\int dP \exp(iPx)\hat{B}_P$ as the Fourier transform of the dressed operators such that $\langle\Phi|\hat{B}_x^\dagger \hat{B}_x|\Phi\rangle = (2\pi)^{-1}\int\int dP_1 dP_2 \exp[-i(P_1 - P_2)x]\langle\Phi|\hat{B}_{P1}^\dagger \hat{B}_{P2}|\Phi\rangle$ could be interpreted as the spatial probability density. As the dressed states $|P\rangle$ contain various bare fermionic momenta p and occupied bosonic modes, the distribution $\langle\Phi|\hat{b}_x^\dagger \hat{b}_x|\Phi\rangle$ can be different from the true physical distribution $\langle\Phi|\hat{B}_x^\dagger \hat{B}_x|\Phi\rangle$. It turns out that the difference between the bare and dressed distributions is significant only for spatially narrow states.

In Fig. 1 we show the difference between the spatial distributions based on $\langle\Phi|\hat{B}_x^\dagger \hat{B}_x|\Phi\rangle$ and $\langle\Phi|\hat{b}_x^\dagger \hat{b}_x|\Phi\rangle$ for the same state. The physical representation $\langle\Phi|\hat{B}_x^\dagger \hat{B}_x|\Phi\rangle$ can be arbitrarily narrow with a width given by Δ. The bare representation, however, takes a finite width even in the limit $\Delta \to 0$. The data in the figure are taken for $\Delta = 0.004$ a.u., which is smaller than the fermion's bare (reduced) Compton wavelength $[1/(Mc) = 0.0073$ a.u.]. It is clear that the bare

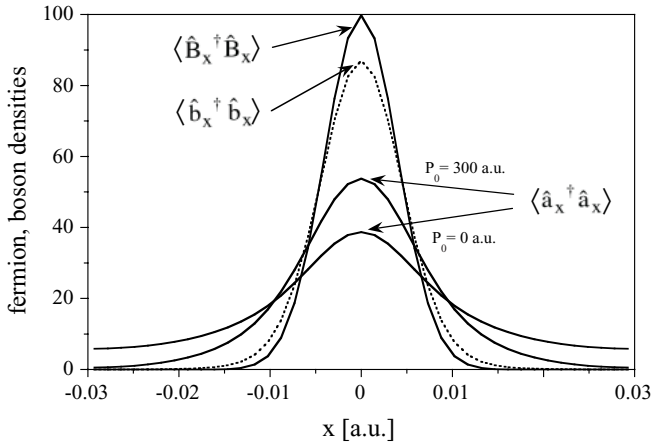

FIG. 1. The spatial distributions of a physical fermion state $|\Phi\rangle = \int dPG(P)|P\rangle$ as defined in Eq. (6). The continuous line is the distribution with respect to the dressed particles, $\langle \hat{B}_x^\dagger \hat{B}_x \rangle$. The dotted line corresponds to the distribution with respect to the bare fermions, $\langle \hat{b}_x^\dagger \hat{b}_x \rangle$. The wider graphs are the corresponding distribution of the bosons $\langle \hat{a}_x^\dagger \hat{a}_x \rangle$ in the state $|\Phi\rangle$ for the central fermion momenta $P_0 = 0$ and $P_0 = 300$ a.u. ($x_0 = 0$, $\Delta = 0.004$ a.u., $\gamma = 0.5$ a.u., bare fermion mass $M = 1$ a.u., bare boson mass $m = 0.2$ a.u., the numerical box length was $L = 0.06$ a.u., $P = 20$, $K = 8$, and the maximum bosonic occupation number of all modes combined was $N = 3$, corresponding to 46,740 states in this Hilbert space).

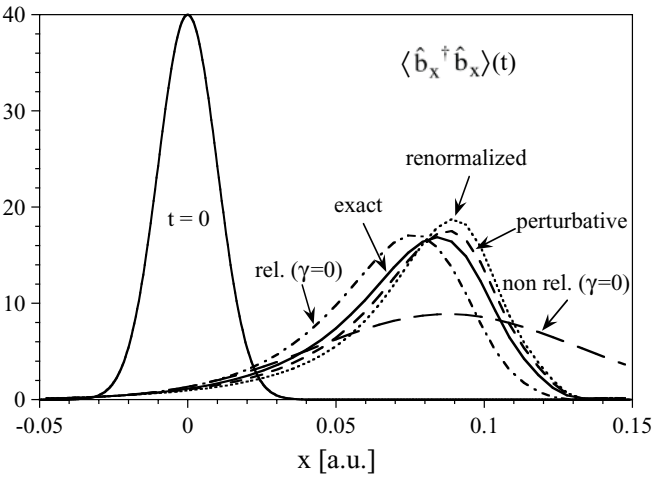

FIG. 2. The spatial distribution of the time-evolved density $\langle \hat{b}_x^\dagger \hat{b}_x \rangle$ at time $t = 8.76 \times 10^{-4}$ a.u. given initially by $|\Phi(t=0)\rangle = \int dPG(P)|P\rangle$ as defined in Eq. (6) with $P_0 = 100$ a.u, $x_0 = 0$, and $\Delta = 0.01$ a.u. For comparison, we accompany the exact distribution with four other graphs: the relativistic and nonrelativistic evolution of the corresponding states for $\gamma = 0$, a state based on the first-order perturbation theory of Eq. (2), evolved with energies given by Eq. (3), and a state based on the evolution of a particle with mass M_{ren} of Eq. (4) (same parameters as in Fig. 1, except $L = 0.2$ a.u.).

representation leads to a wider distribution. The two graphs show the corresponding distribution of the dressing bosons. While the fermion's distribution is independent of the central momentum P_0, the dressing bosons' distribution is widest for a physical fermion at rest ($P_0 = 0$). From a purely classical electrodynamical point of view, the dressing bosons could be loosely associated with the electric field created by the charged fermion. It is known that the longitudinal field of a rapidly moving charged particle is reduced in the forward and backward directions [16]. Our observed narrowing of the boson's distribution for faster fermions could be viewed as reminiscent of this classical field effect. The total number of dressing bosons, computed as $\int dx \langle \Phi | \hat{a}_x^\dagger \hat{a}_x | \Phi \rangle = 0.95$, is similar for $P_0 = 0$ and $P_0 = 300$ a.u. In other words, our chosen coupling strength $\gamma = 0.5$ a.u. is so strong that the bare fermion requires almost a whole boson to become dressed.

As the initial fermion state is a superposition of states with different momenta P, its spatial distribution spreads out. In Fig. 2 we graph the initial spatial density of the physical fermion. It has an initial spatial width $\Delta(t=0) = 0.01$ a.u. and its momentum distribution is centered around $P_0 = 100$ a.u. The width Δ is sufficiently large such that the initial distribution is similar to the distribution of the corresponding bare particle. The graph shows various final states associated with the time $t = 8.76 \times 10^{-4}$ a.u. In order to set the scale, the rightmost graph shows the packet if the time evolution were nonrelativistic, formally associated with $c = \infty$. As expected, this wave packet spreads symmetrically while its center moves from $x_0 = 0$ to $x = 0.0876$ a.u. The wave packet that has moved by the least distance is associated with the fully relativistic time evolution in the absence of any coupling ($\gamma = 0$). As the spreading of the front edge is less than that of the trailing edge, the packet evolves into an asymmetric shape. The location of the peak is about $x = 0.0744$ a.u., suggesting an effective velocity of $v = 84.9$ a.u., consistent with the velocity $c^2 P/\sqrt{(M^2c^4 + c^2P^2)}$, which amounts to 80.8 a.u. describing a monochromatic beam with $P = 100$ a.u.

The graph depicted by a continuous line denotes the wave packet following the true dynamics of the physical particle for a coupling of $\gamma = 0.5$ a.u. Note that the peak is located at $x = 0.0841$ a.u., which suggests a larger value of the effective velocity ($v = 96.1$ a.u.) than for the $\gamma = 0$ case. In other words, the physical particle evolves as if its effective mass were smaller than its bare mass M. If we convert the velocity $v = 96.1$ a.u. and $P = 100$ a.u. to the corresponding mass via $M = p\sqrt{(v^{-2} - c^{-2})}$, we find $M(\gamma = 0.5 \text{ a.u.}) = 0.742$ a.u., which is 26% less than the bare mass. We will comment in more detail below on the evolution of the spatial width.

The remaining graphs are the final states obtained analytically under the assumption that the dynamics can be approximated by second-order perturbation theory in γ with regard to the energy. For $\gamma < 0.3$ a.u. (not shown), both graphs based on Eqs. (2) and (4) agree with the exact (numerical) distribution indicating the largest value of γ (roughly 0.3 a.u.) for which the dynamics is still perturbative. The figure shows that for $\gamma < 0.5$ a.u. both perturbative approximations overestimate the true velocity and predict a final wave packet that has evolved too far to the right.

Let us now examine this dressing-induced velocity increase in more detail and how it depends on the parameters. Following the usual Hamiltonian equations of motion, the velocity is given by the derivative of the energy with respect to the canonical momentum, $v = \partial E(P)/\partial P$. In Fig. 3

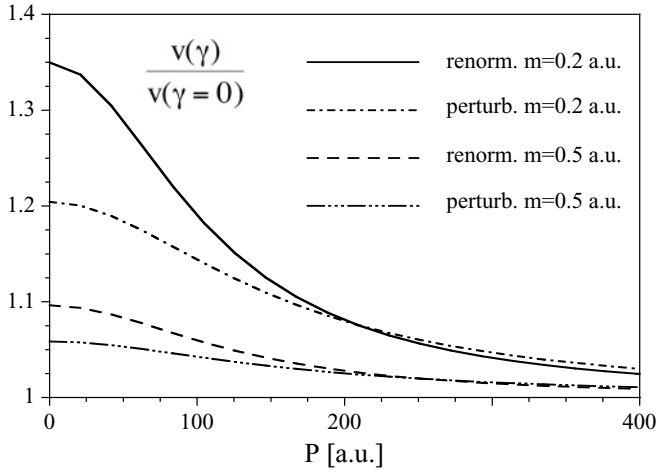

FIG. 3. The velocity enhancement factor due to boson dressing, defined by the ratio of the true physical velocity $\partial E(p,\gamma)/\partial p$ associated with the momentum p and the velocity in the absence of any coupling, $\partial E(p,\gamma=0)/\partial p = pc^2/\sqrt{(M^2c^4+p^2c^2)}$.

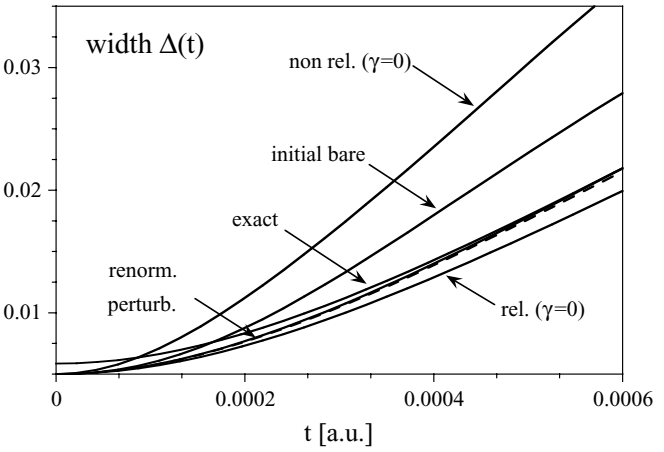

FIG. 4. The time evolution of the spatial width $\Delta(t)$ for a bare and dressed fermion, for a nonrelativistic and relativistic particle for $\gamma = 0$, and for the state computed perturbatively and via mass renormalization. The coupling is $\gamma = 0.5$ a.u., and the bare fermion and boson masses are $M = 1$ a.u. and $m = 0.2$ a.u. (numerical parameters as in Fig. 2).

we graph the dressing-induced velocity enhancement factor, $[\partial E(P,\gamma)/\partial P]/[\partial E(P,\gamma=0)/\partial P]$, as a function of the momentum P for two different boson masses m. We see that a smaller boson mass leads to larger velocity increase. States with larger canonical momentum lead to less of a velocity increase. However, for asymptotically large momentum, the ratio has to approach unity, as $\partial E(P)/\partial P$ approaches c independent of γ and P. The coupling $\gamma = 0.5$ a.u., bare fermion mass $M = 1$ a.u., and two values of the bare boson mass are indicated in the figure.

Let us now analyze the spatial spreading of the distributions shown in Fig. 2 in more detail. We can characterize this spreading by computing the time evolution of the spatial width $\Delta(t)^2 = \langle x(t)^2\rangle - \langle x(t)\rangle^2$.

There are two competing effects in which the reduction of the effective mass due to boson dressing can modify the evolution of the spatial width. First, for a fixed momentum, an effectively smaller mass leads to a larger velocity compared to the bare particle ($\gamma = 0$). While for nonrelativistic speeds the spatial spreading does not depend on the average velocity of the wave packet, in the relativistic regime this spreading decreases with increasing velocity [17,18]. In fact, a wave packet that evolves with the speed of light does not increase its spatial width at all. Due to this relativistic suppression, one could expect that the (faster) physical fermion wave packet should spread less than its bare counterpart. This prediction could be consistent with the fact that the observed peak height of the physical fermion is indeed larger than the bare particle's height (not shown in the figure). On the other hand, there is a second (nonrelativistic) mechanism that would predict a larger amount of spreading. It is based on the fact that the dispersion in the velocity (and not in the momentum) is the actual source for the spatial spreading. If we equate the momentum width of the bare and dressed fermion (as we did in our comparison in the figure), it is obvious that the dressed fermion has a larger velocity uncertainty. As a result, this mechanism by itself would predict an increase of the spatial spreading due to the dressing. A more detailed analysis is therefore required to see which mechanism dominates. In Appendix C we show how the spatial width is related to the momentum dependence of the energy in the fully coupled relativistic regime.

In Fig. 4 we compare the predictions for the different spreading behavior of the fermion density $\langle \hat{b}_x^\dagger \hat{b}_x\rangle$ for six different scenarios. We also include the corresponding predictions of first-order perturbation theory and the renormalization technique. As pointed out earlier, the numerical value of the coupling $\gamma = 0.5$ a.u. is relatively strong, such that the bare fermion requires nearly an entire boson to get dressed ($\int dk \langle \hat{a}_k^\dagger \hat{a}_k\rangle = 0.95$).

The width according to the nonrelativistic calculation is $\Delta^2(t) = \Delta^2 + t^2/(4\Delta^2)$, which grows faster than the relativistic widths. The next largest width is associated with the time evolution of an initially bare fermion for $\gamma = 0.5$ a.u. This large width could be associated with the unavoidable sequence of recoils this particle experiences as it emits (and probably also reabsorbs) the bosons. While the prediction according to the perturbative energy as well as the renormalization technique agree well with the exact width, the width of the time evolution for $\gamma = 0$ is less than the other predictions. The slight offset of the initial width for $t = 0$ is related to the difference between $\langle \hat{b}_x^\dagger \hat{b}_x\rangle$ (used in Fig. 4) and $\langle \hat{B}_x^\dagger \hat{B}_x\rangle$ as shown in Fig. 1. The exact graph shows that, among the two competing mechanisms outlined above, the width increase due to the relativistic spreading dominates the quantum-field-theoretical spreading reduction due to its larger velocity.

One could attempt to associate the various spreading behaviors with different effective masses. While the renormalization technique describes the entire spectrum with a single (coupling-dependent) mass, it is nontrivial to uniquely associate a value of such a quantity to the perturbative energies. For the upper range of validity of perturbation theory ($\gamma = 0.3$ a.u., $M = 1$ a.u., and $m = 0.2$ a.u.), the renormalized mass is about 10% less than the bare mass, $M_{\rm ren} = 0.907$ a.u. There are various ways in which one can also use

the perturbative solution $E(P,\gamma)$ from Eq. (3) to compute a mass. While for the usual energy-momentum relationship $E(P) = (M^2c^4 + c^2P^2)^{1/2}$ the terms $E(P=0)/c^2$ and $[\partial^2 E(P)/\partial P^2|_{P=0}]^{-1}$ are exactly identical and equal to M, in perturbation theory we obtain $E(P=0,\gamma)/c^2 = 0.907$ a.u. and a similar value for $[\partial^2 E(P,\gamma)/\partial P^2|_{P=0}]^{-1} = 0.932$ a.u. If we take the exact eigenenergy we can directly compute $E(P = 0,\gamma = 0.3 \text{ a.u.})/c^2 = 0.908$ a.u., supporting the validity of the perturbation and renormalization approaches for $\gamma < 0.3$ a.u.

In order to see nonperturbative effects and deviations from the usual energy-momentum relationship, we have to increase the coupling constant to $\gamma = 0.5$ a.u. The exact value of the mass obtained from the numerical energy eigenvalues is now $E(P=0,\gamma)/c^2 = 0.753$ a.u. While the renormalized technique predicts the mass $M_{\text{ren}} = 0.741$ a.u. and therefore underestimates the true mass, the eigenvalues $E(P,\gamma)$ obtained by perturbative theory lead to $E(P=0,\gamma)/c^2 = 0.740$ a.u. and $[\partial^2 E(P,\gamma)/\partial P^2|_{P=0}]^{-1} = 0.832$ a.u. The incompatibility of the last two estimates suggests deviations from the usual energy-momentum relationship. The difference between 0.753 and 0.740 a.u. suggests a relative error of 1.7% for second-order perturbation theory.

It might be an interesting question to explore how an initially bare fermion with central momentum p_0 loses its mass as it evolves into a physical particle. Does the bare fermion accelerate to obtain the larger speed associated with its smaller mass? Is this acceleration accomplished by emitting more bosons into the backward direction? We have computed $\langle x(t)\rangle$ for this case and found almost no acceleration. This can be understood best within a framework based on dressed states. In this basis, the initial bare state of the fermion is a superposition of a physical fermion (that together with its dressing bosons evolves with its fast velocity with mass M_{ren}) and excess bosons that escape to $\pm\infty$ as the state evolves.

We should note that due to the relatively narrow initial width Δ, the spreading is relativistic. For comparison, a nonrelativistic calculation [obtained from Eq. (C7) for $c \to \infty$) for $\gamma = 0$ would predict $\sigma^2 = 1/(2M\Delta)^2 = 2500$ a.u., whereas the relativistic spreading rate from Eq. (C6) is only $\sigma^2 = 1867$ a.u. For the smaller coupling, $\gamma = 0.3$ a.u., the exact spreading rate can be obtained by approximating the derivative with respect to the momentum via the symmetric finite-difference formula, $\partial E(P,\gamma)/\partial P \approx (E_{p+\Delta p} - E_{p-\Delta p})/(2\Delta p)$, and using this expression in Eq. (C4b) we obtain $\sigma^2 = 2083$ a.u., which differs by less than 4% from the perturbative (2095 a.u.) and the renormalized (2166 a.u.) values. Again, nonperturbative effects become apparent for $\gamma = 0.5$ a.u., for which the true spreading rate even amounts to $\sigma^2 = 2385$ a.u., whereas both the perturbative (2535 a.u.) and renormalization (2892 a.u.) approaches overestimate this rate. We should also mention that if the coupling function in the Hamiltonian [9,10] were chosen to be $\Gamma(p,k) \equiv (4\pi\omega_k)^{-1/2}$, the dressed fermion would evolve with a smaller velocity than its bare analog, suggesting a larger effective mass, if it can be defined.

IV. DISCUSSION

We have analyzed the composition of a localized physical particle in terms of its bare and dressed fermionic and bosonic states. We found the surprising result that, independent of the fermion's momentum, the corresponding dressing bosons typically have very small momenta but nevertheless can evolve with the same velocity as the fermion. We compared the space-time evolution of a physical particle with that of its bare counterpart and showed the importance of using dressed observables. The time evolution of the center of mass and the wave packet's spatial width suggests that the physical particle effectively has a lower mass than its corresponding bare particle and therefore moves faster for a given momentum.

In this work we have outlined the tools for the next step to simulate the interaction of a physical fermion with a boson wave packet with space-time resolution. It might be interesting to examine the role the dressing bosons play with regard to the way the fermion absorbs and re-emits a boson. Our preliminary results for this Compton scattering [19] indicate that, for those values of the coupling γ for which our numerical approach is feasible, the corresponding (Klein-Nishina-type) cross sections are very small such that the dressing photons associated with the transmitted fermion are much more dominant than the reflected bosons. As the dressing bosons are characterized by only very small bare momenta and therefore differ from the incoming boson momentum, a corresponding analysis in momentum space might lead to results that are easier to interpret.

ACKNOWLEDGMENTS

We thank Professor C. C. Gerry for many useful discussions and suggesting this work. We also appreciate several helpful discussions with Professor S. Hassani. This work has been supported by the NSF. We also acknowledge support from the Research Corporation.

APPENDIX A

Here we show that in a spatially localized physical fermion the dressing bosons are glued to the bare fermion independent of their momenta k. We assume that the physical fermion is given by the expansion $|\Phi(t)\rangle = \int dP G(P,t)|P\rangle$, where the amplitude for the total momentum state is given by $G(P,t) = (2/\pi)^{1/4}\Delta^{1/2}\exp[-(P - P_0)^2\Delta^2]\exp(-iPx_0)\exp[-iE(P)t]$. We further assume that the energy eigenstate $|P\rangle$ is given by the first-order perturbative expansion $|P\rangle = |P\rangle + \int dk C(p,k)|p-k,n_k = 1\rangle$, where the precise form of the real expansion coefficient $C(p,k)$ is given by Eq. (2). We also assume that the energy $E(P)$ is given either by the perturbative expansion, Eq. (3), or by the expression based on the Feynman graphs for the renormalized mass, Eq. (4).

In order to compute the time evolution of the average position of the bosonic portion of the state $|\Phi(t)\rangle$, we first have to express the bosonic position operator $\hat{X}_b \equiv \int dx x \hat{a}_x^\dagger \hat{a}_x$ in terms of the usual bare momentum annihilation and creation operators $\hat{a}_k$ and $\hat{a}_k^\dagger$. We insert the definitions into the expression for $\hat{X}_b$ and obtain $\hat{X}_b = (2\pi)^{-1}\iiint dx\, dk_1\, dk_2\, x\, \hat{a}_{k1}^\dagger \hat{a}_{k2}\exp[i(k_2 - k_1)x]$. Now we introduce new variables $k \equiv (k_2 - k_1)/2$ and $K \equiv (k_2 + k_1)/2$ such that we can perform the integration over x,

$\int dx x \exp(i2kx) = (-\pi i/2)\partial\delta(k)/\partial k$. If we then integrate by parts and evaluate the integral over k, we obtain

$$\hat{X}_b = (i/2)\partial \left(\int dK \hat{a}^\dagger_{K-k}\hat{a}_{K+k} \right) \Big/ \partial k|_{k=0}. \quad \text{(A1)}$$

The same expression can be obtained for the (bare) fermionic position operator; we just have to replace $\hat{a}_k$ with $\hat{b}_p$.

Next we calculate the scalar product

$$\langle\Phi(t)|\hat{X}_b|\Phi(t)\rangle = (i/2)\partial \left[\int dK \langle\Phi(t)|\hat{a}^\dagger_{K-k}\hat{a}_{K+k}|\Phi(t)\rangle \right] \Big/ \partial k|_{k=0}. \quad \text{(A2)}$$

If we insert the expansion of the state $|\Phi(t)\rangle$ in terms of the bare states, we obtain

$$\langle\Phi(t)|\hat{X}_b|\Phi(t)\rangle = (i/2)\partial \Big[\int\int\int\int\int\int dK\, dp_1\, dp_2\, dk_1\, dk_2 \times G^*(p_1,t)G(p_2,t)C(p_1,k_1)C(p_2,k_2) \times A(p_1,p_2,k_1,k_2,K,k) \Big] \Big/ \partial k|_{k=0}, \quad \text{(A3)}$$

where the matrix element $A(p_1,p_2,k_1,k_2,K,k) \equiv \langle p_1 - k_1, n_{k1} = 1|\hat{a}^\dagger_{K-k}\hat{a}_{K+k}|p_2 - k_2, n_{k2} = 1\rangle$ is just a product of three Dirac delta functions: $A = \delta(k_2 - K - k)\delta(k_1 - K + k)\delta(p_1 - p_2 + 2k)$. As a result, three of the five integrals can be solved, leading to

$$\langle\Phi(t)|\hat{X}_b|\Phi(t)\rangle = (i/2)\partial \Big[\int dp G(p-2k,t)^* G(p,t) \times \int dK C(p-2k,K-k)C(p,K+k) \Big] \Big/ \partial k|_{k=0}. \quad \text{(A4)}$$

As the integration over p extends from $-\infty$ to ∞, we can shift the integration variable p to $p + k$. For any function $f(x)$, we have $\partial[f(x-k)f(x+k)]/\partial k|_{k=0} = 0$ for any x, so we only have to compute the derivative of $G^*(p-k,t)G(p-k,t)$ when we apply the product rule to differentiate the four factors. For the special case of our Gaussian functions defined above, we can split off the exponential time factor and obtain

$$(i/2)\partial[G^*(p-k,t)G(p+k,t)]/\partial k|_{k=0} = [t\partial E(p)/\partial p + x_0]|G(p,t=0)|^2. \quad \text{(A5)}$$

Using this expression we obtain for the scalar product the remarkably simple form

$$\langle\Phi(t)|\hat{X}_b|\Phi(t)\rangle = \int dp[t\partial E(p)/\partial p + x_0]|G(p)|^2 \times \int dK C(p,K)^2. \quad \text{(A6)}$$

If the Gaussian distribution $G(p)$ is narrowly centered around $p = p_0$ (corresponding to a large spatial width Δ), we can approximate this factor with $\partial E(p_0)/\partial p_0$ (the velocity of the physical fermion), leading to $\langle\Phi(t)|\hat{X}_b|\Phi(t)\rangle = [t\partial E(p_0)/\partial p_0 + x_0]N_b$. The factor

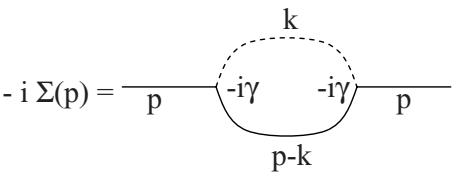

FIG. 5. One-loop correction to the two-point Green's function.

$N_b \equiv \int dp|G(p)|^2 \int dK C(p,K)^2$ denotes the total number of bosons in the state $|\Phi\rangle, N_b = \int dk \langle\Phi|\hat{a}^\dagger_k\hat{a}_k|\Phi\rangle = \int dx \langle\Phi|\hat{a}^\dagger_x\hat{a}_x|\Phi\rangle$. In order to convert the scalar product $\langle\Phi(t)|\hat{X}_b|\Phi(t)\rangle$ into the average value of the bosonic position (denoted by $\langle X_b\rangle = \langle\Phi|\hat{X}_b|\Phi\rangle/N_b$), we have to divide this value by the overall norm of the boson distribution. We obtain the final result,

$$\langle X_b\rangle = x_0 + \partial E(p_0)/\partial p_0 t, \quad \text{(A7)}$$

which shows that the bare bosons' average position changes precisely in the same way as the bare fermion. The dressing bosons are glued to the bare fermion even completely independently of the distribution of the bare bosons as given by $C(p,k)$, which is a maximum for bosons with $k = 0$.

APPENDIX B

The renormalized mass can be computed perturbatively [3] starting with the one-loop correction to the two-point (momentum-space) Green's function, shown in Fig. 5.

The loop integral $-i\Sigma(p)$ is

$$-i\Sigma(p) = [1/(2\pi)^2] \int d^2k\, i/(k^2 - m^2c^2) \times i[\gamma^\mu(p_\mu - k_\mu) + Mc]/[(p-k)^2 - M^2c^2] \quad \text{(B1)}$$

Here p and k are space-time two-vectors $p_\mu = (E/c, \mathbf{p})$ and $k_\mu = (\omega/c, \mathbf{k})$, where the bold-faced $\mathbf{p}$ and $\mathbf{k}$ are the ordinary spatial momenta. The signature of the Minkowski metric has been chosen such that $p^2 = (E/c)^2 - \mathbf{p}^2$. This integral is actually convergent in one spatial dimension and therefore renormalization will yield a finite correction to the mass. By introducing a Feynman parameter, $1/(AB) = \int_0^1 dz/[zA + (1-z)B]^2$, the loop integral can be evaluated by completing the square in the denominator, giving

$$\begin{aligned}\Sigma(p) &= [\gamma^2/(4\pi)] \int_0^1 dz (z\gamma^\mu p_\mu + Mc)/[z(1-z)p^2 - zm^2c^2 - (1-z)M^2c^2] \\ &= \gamma^2/(4\pi)\{-\gamma^\mu p_\mu/p^2 \ln(m/M) + 1/q[2Mc + \gamma^\mu p_\mu(p^2 - m^2c^2 + M^2c^2)/p^2] \\ &\quad \times \{\tan^{-1}[(-p^2 - m^2c^2 + M^2c^2)/q] - \tan^{-1}[(p^2 - m^2c^2 + M^2c^2)/q]\}\},\end{aligned} \quad \text{(B2)}$$

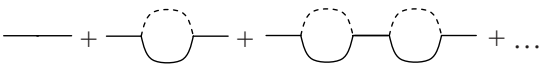

FIG. 6. Sum over one-loop contributions to the two-point Green's function.

where $q \equiv \sqrt{[4p^2M^2c^2 - (p^2 - m^2c^2 + M^2c^2)^2]}$. As shown in Fig. 6, the perturbative expansion of the two-point Green's function $G_2(p)$ will contain terms with multiple copies of the one-particle irreducible diagram (Fig. 5). Summing up over all these contributions gives

$$\begin{aligned} G_2(p) &= i/(\gamma^\mu p_\mu - Mc) + i/(\gamma^\mu p_\mu - Mc)[-i\Sigma(p)] \\ &\quad \times i/(\gamma^\mu p_\mu - Mc) + i/(\gamma^\mu p_\mu - Mc)[-i\Sigma(p)] \\ &\quad \times i/(\gamma^\mu p_\mu - Mc)[-i\Sigma(p)]i/(\gamma^\mu p_\mu - Mc) + \cdots \\ &= i/[\gamma^\mu p_\mu - Mc - \Sigma(p)]. \end{aligned} \tag{B3}$$

The pole of this propagator occurs at the renormalized mass M_{ren}. We must also include the effects of the wave function renormalization, $\psi_{\text{ren}} = \sqrt{Z}\psi$. Therefore, Z and M_{ren} must be found such that $G_2^{-1}(p) = Z[\gamma^\mu p_\mu - Mc - \Sigma(p)] = \gamma^\mu p_\mu - M_{\text{ren}}c$ when evaluated at $p^2 = M_{\text{ren}}^2c^2$. The wave function renormalization factor Z can be found by equating powers of $\gamma^\mu p_\mu$, and then M_{ren} can be evaluated as

$$\begin{aligned} M_{\text{ren}} &= M - \gamma^2/(4\pi M)[\ln(m/M) + \sqrt{(4M^2 - m^2)}/m \\ &\quad \times \big(\tan^{-1}[m/\sqrt{(4M^2 - m^2)}] \\ &\quad + \tan^{-1}\{(2M^2 - m^2)/[m\sqrt{(4M^2 - m^2)}]\}\big)]. \end{aligned} \tag{B4}$$

APPENDIX C

Here we show how the spatial width Δ changes as a function of time. As Δ is given by $\Delta(t)^2 = \langle x(t)^2\rangle - \langle x(t)\rangle^2$, we need to calculate first $\langle x(t)^2\rangle = \langle\Phi(t)|x^2|\Phi(t)\rangle$. This is given by

$$\begin{aligned} \langle x(t)^2\rangle &= (2\pi)^{-1}\int\int\int dx\, dp_1\, dp_2 G^*(P_1)G(P_2)x^2 \\ &\quad \times \exp[-i(P_1 - P_2)x]\exp\{-i[E(P_1) - E(P_2)]t\}. \end{aligned} \tag{C1}$$

We can now use this expression to show how the temporal growth of the width depends on the momentum dependence of the energy eigenvalues $E(P)$. First we define new momentum variables, $P \equiv (P_1 + P_2)/2$ and $p \equiv (P_1 - P_2)/2$, and abbreviate the energy exponent by $D(P,p) \equiv E(P + p) - E(P - p)$. Using $x^2\exp(-i2px) = -\frac{1}{4}\partial^2\exp(-i2px)/\partial p^2$, we can integrate Eq. (C1) twice by parts with respect to the variable p. The spatial integration can be performed, $\int dx\exp(-i2px) = \pi\delta(p)$, which then simplifies the integration over p, leading to the single integral

$$\begin{aligned} \langle x(t)^2\rangle &= -\tfrac{1}{4}\int dP\partial^2\{G^*(P - p)G(P + p) \\ &\quad \times \exp[-iD(P,p)t]\}/\partial p^2|_{p=0}, \end{aligned} \tag{C2}$$

where the second derivative needs to be evaluated at $p = 0$. If we then insert the specific Gaussian form of the momentum expansion amplitude, $G(P) = (2/\pi)^{1/4}\Delta^{1/2}\exp[-(P - P_0)^2\Delta^2]$, the product $G^*(P - p)G(P + p)$ factorizes, and we obtain

$$\begin{aligned} \langle x(t)^2\rangle &= -\frac{1}{4}(2/\pi)^{1/2}\Delta\int dP\exp[-2(P - P_0)^2\Delta^2] \\ &\quad \times \partial^2\exp[-2p^2\Delta^2 - iD(P,p)t]/\partial p^2|_{p=0}. \end{aligned} \tag{C3}$$

The second derivative with respect to p can be performed, leading to the expression $\partial^2\exp[-2p^2\Delta^2 - iD(P,p)t]/\partial p^2|_{p=0} = -4\Delta^2 - \{\partial[E(P + p) - E(P - p)]/\partial p|_{p=0}\}^2t^2$. This term can be simplified further to the final expression

$$\langle x(t)^2\rangle = \Delta^2 + \sigma^2t^2, \tag{C4a}$$

$$\sigma^2 \equiv (2/\pi)^{1/2}\Delta\int dP\exp[-2(P - P_0)^2\Delta^2][\partial E(P)/\partial P]^2. \tag{C4b}$$

The derivation to compute $\langle x(t)\rangle = \langle\Phi(t)|x|\Phi(t)\rangle$ involves a very similar sequence of steps as the above derivation and leads first to

$$\begin{aligned} \langle x(t)\rangle &= -(i/2)\int dP\partial\{G^*(P - p)G(P + p) \\ &\quad \times \exp[-iD(P,p)t]\}/\partial p|_{p=0}. \end{aligned} \tag{C5}$$

The derivative with respect to p can be performed, leading to the expression $\partial\{\exp[-2p^2\Delta^2 - iD(P,p)t]\}/\partial p|_{p=0} = -2i\partial E(P)/\partial Pt$. This term can be simplified further to the final expression $\langle x(t)\rangle = (2/\pi)^{1/2}\Delta\int dP\partial E(P)/\partial P\exp[-2(P - P_0)^2\Delta^2]t = \int dP|G(P)|^2\partial E(P)/\partial Pt$, which vanishes unless $P_0 \neq 0$.

For $P_0 = 0$, the source term in Eq. (C4b) for the spatial spreading σ^2 has quite an interesting interpretation. As in a Hamiltonian formalism, the derivative $\partial E(P)/\partial P$ is the kinetic velocity dx/dt, and therefore the term σ^2 resembles the average value of the velocity squared. However, it is integrated over a Gaussian distribution of its corresponding canonical momentum P, so it is not just the simple variance of the kinetic velocity as one could expect from nonrelativistic considerations.

To give a simple example, the expression for σ^2 takes a more familiar form if we approximate the eigenvalue by one that corresponds to a free particle, $E(P) = (M^2c^4 + c^2P^2)^{1/2}$. For $P_0 = 0$, the resulting integral can be performed analytically in the form of the error function $\text{erf}(x)$:

$$\sigma^2 \equiv \exp(2M^2c^2\Delta^2)c^3M^2(2\pi)^{1/2}\Delta[\text{erf}(\sqrt{2Mc\Delta}) - 1] + c^2. \tag{C6}$$

The key parameter is apparently the ratio of the fermion's initial width Δ and the Compton wavelength $1/(Mc)$. If we now use the asymptotic (large c) expansion for the error function, we obtain as the leading terms

$$\begin{aligned} \sigma^2 &\equiv 1/(2M\Delta)^2 + 3/16c^2/(Mc\Delta)^4 \\ &\quad - 15/64c^2/(Mc\Delta)^6 + \cdots. \end{aligned} \tag{C7}$$

The first term is obviously the usual (nonrelativistic) variance of the velocity, fulfilling the Heisenberg uncertainty relationship. The following terms are the relativistic corrections to the wave-packet spreading. We note that the spreading speed defined as σ ranges from its lowest value, $1/(2M\Delta)^2$, to its largest value, c.

The general dependence of the energy eigenvalue on the total momentum P must be obtained numerically, but it can be approximated by its perturbative form shown in Eq. (3). As the spreading given by σ depends on the derivative $\partial E(P)/\partial P$, the $k = 0$ term from the perturbative sum (independent of P) does not contribute. If we insert the expressions of either Eq. (4) or Eq. (5) into Eq. (C4b), we can compute the impact of the coupling γ on the spreading rate.

[1] For a review, see, e.g., S. S. Schweber, *An Introduction to Relativistic Quantum Field Theory* (Harper & Row, New York, 1962).
[2] See, e.g., C. Itzykson and J. Zuber, *Quantum Field Theory* (McGraw-Hill, New York, 1980).
[3] M. E. Peskin and D. V. Schroeder, *An Introduction to Quantum Field Theory* (Westview Press, Boulder, 1995).
[4] E. V. Stefanovich, *Relativistic Quantum Dynamics: A Non-traditional Perspective on Space, Time, Particles, Fields, and Action-at-a-Distance* (Mountain View, 2004), e-print arXiv:physics/0504062v10 [physics.gen-ph].
[5] T. Cheng, Q. Su, and R. Grobe, Opt. Commun. **283**, 1008 (2010).
[6] E. V. Stefanovich, Ann. Phys. **292**, 139 (2001).
[7] E. V. Stefanovich, e-print arXiv:hep-th/0503076.
[8] T. Cheng, E. R. Gospodarczyk, Q Su, and R. Grobe, Ann. Phys. **325**, 265 (2010).
[9] O. W. Greenberg and S. S. Schweber, Nouvo Cimento **8**, 378 (1958).
[10] R. Walter, Nouvo Cimento A **68**, 426 (1970).
[11] T. Cheng, C. C. Gerry, Q. Su, and R. Grobe, Europhys. Lett. **88**, 54001 (2009).
[12] L. I. Schiff, *Quantum Mechanics* (McGraw-Hill, New York, 1949).
[13] L. Mandel and E. Wolf, *Optical Coherence and Quantum Optics* (Cambridge University, New York, 1995).
[14] C. C. Gerry and P. L. Knight, *Introductory Quantum Optics* (Cambridge University, Oxford, 2004).
[15] W. P. Schleich, *Quantum Optics in Phase Space* (Springer-Verlag, Berlin, 2001).
[16] J. D. Jackson, *Classical Electrodynamics* (Wiley, New York, 1999).
[17] Q. Su, B. A. Smetanko, and R. Grobe, Laser Phys. **8**, 93 (1998).
[18] Q. Su, B. A. Smetanko, and R. Grobe, Opt. Express **2**, 277 (1998).
[19] R. E. Wagner, Q. Su, and R. Grobe, Phys. Rev. A **82**, 022719 (2010).